Mon. Not. R. Astron. Soc. **000**, 1–5 (2005) Printed 1 February 2008 (MN LATEX style file v2.2)

X-ray reflection in accreting stellar-mass black hole systems

R. R. Ross[1⋆] and A. C. Fabian[2]
[1]*Physics Department, College of the Holy Cross, Worcester, MA 01610, USA*
[2]*Institute of Astronomy, Madingley Road, Cambridge CB3 0HA*

1 February 2008

ABSTRACT
The X-ray spectra of accreting stellar-mass black hole systems exhibit spectral features due to reflection, especially broad iron Kα emission lines. We investigate the reflection by the accretion disc that can be expected in the high/soft state of such a system. First, we perform a self-consistent calculation of the reflection that results from illumination of a hot, inner portion of the disc with its atmosphere in hydrostatic equilibrium. Then we present reflection spectra for a range of illumination strengths and disc temperatures under the assumption of a constant-density atmosphere. Reflection by a hot accretion disc differs in important ways from that of a much cooler disc, such as that expected in an active galactic nucleus.

Key words: accretion, accretion discs – black hole physics – line: formation – radiative transfer – X-rays: binaries

1 INTRODUCTION

Studies of the spectra of accreting black holes are important for understanding the accretion flow and geometry, and hence the effects of strong gravity and black-hole spin. In a black-hole binary (BHB) system, radiatively efficient accretion through a disc generates a quasi-thermal spectrum which is well seen in the high/soft states (see Remillard & McClintock 2006). Modeling of such spectra, with detailed attention paid to spectral hardening by radiation-transfer effects, has been undertaken by Shimura & Takahara 1995, Merloni, Fabian & Ross 2000, and recently by Davis and collaborators (Davis et al. 2005; Davis & Hubeny 2006). At the same time, coronal emission in such sources generates a power-law spectrum by inverse Compton scattering of the thermal disc photons. This hard emission can irradiate the disc to produce a reflection spectrum (Guilbert & Rees 1988; Lightman & White 1988; George & Fabian 1991; Ross & Fabian 1993) which may contain sharp spectral features that can reveal the velocity of the matter and the depth of the gravitational well (Fabian et al. 2000; Reynolds & Nowak 2003; Miller 2007).

Here we investigate reflection spectra in BHBs. Broad iron emission lines have been found in a wide range of BHBs (Bałucińska-Church & Church 2000; Martocchia et al. 2002; Miller et al. 2002a,b,c; Miller et al. 2004; Miniutti, Fabian & Miller 2004; Rossi et al. 2005; Miller et al 2006) indicating the presence of reflection components in those objects, particularly in the very high and the low/hard states. Our previous studies of active galactic nuclei (Ross & Fabian 1993; Ballantyne, Ross & Fabian 2001; Ross & Fabian 2005) concentrated on the irradiation of slabs of gas which would otherwise be cold. For a BHB, however, the gas in the accretion disc is expected to be warm ($T \sim 10^6$ K). Low-Z elements are stripped of electrons even before photoionization by illuminating radiation is considered, and thermal emission by the gas can dominate portions of the X-ray spectrum.

We begin by considering reflection by an accretion-disc surface layer which has a density structure consistent with the condition of hydrostatic equilibrium. We then show a range of spectra produced by constant-density slabs heated from below by blackbody radiation and illuminated from above by hard power-law radiation.

2 ILLUMINATED DISC ATMOSPHERE

2.1 Method

We begin with a model for illumination of gas in hydrostatic equilibrium atop a spatially thin accretion disc. We take the mass of the central black hole to be $M = 10M_\odot$ and the accretion rate to be a fraction $\varepsilon = \dot{M}/\dot{M}_{\rm Edd}$ of the value corresponding to the Eddington limit. If all gravitational energy is dissipated within the disc, the total flux emerging from the disc at radius R (Shakura & Sunyaev 1973) is expected to be

$$F_{\rm disc} = \frac{3GM\dot{M}}{8\pi R^3}\left(1-\sqrt{\frac{R_{\rm min}}{R}}\right). \quad (1)$$

For a nonrotating black hole, $R_{\rm min} = 6R_{\rm g}$, where $R_{\rm g} = GM/c^2$ is the gravitational radius.

We model the radiative transfer and hydrostatic equilibrium throughout a surface layer of total Thomson depth $\tau_{\rm T} = 10$. The base of this surface layer is fixed at height H above the midplane of the disc, where H is the estimate for the half-thickness of the accretion disc given by Merloni et al. (2000). The total flux $F_{\rm disc}$ enters the surface layer from below in the form of a blackbody spectrum.

⋆ rross@holycross.edu

The method for treating the radiative transfer and finding the self-consistent temperature and ionization state of the gas has been described by Ross & Fabian (2005) and references therein. The steady-state radiation field is assumed to satisfy the Fokker-Planck/diffusion equation,

$$\left(\frac{\partial n}{\partial t}\right)_{\rm FP} + \frac{\partial}{\partial z}\left(\frac{c}{3\kappa}\frac{\partial n}{\partial z}\right) + \frac{j_E h^3 c^3}{8\pi E^3} - c\kappa_{\rm A} n \equiv 0\,, \qquad (2)$$

where n is the photon occupation number, E is the photon energy, z is the vertical height above the midplane of the accretion disc, j_E is the spectral emissivity, $\kappa = \kappa_{\rm A} + \kappa_{\rm KN}$ is the total opacity (per volume), $\kappa_{\rm A}$ is the absorption opacity, and $\kappa_{\rm KN}$ is the Klein-Nishina opacity for Compton scattering. The leading term, $(\partial n/\partial t)_{\rm FP}$, is given by the Fokker-Planck equation of Cooper (1971) and accurately treats the effects of Compton scattering for $E \lesssim 1\,{\rm MeV}$ and $kT \lesssim 100\,{\rm keV}$. As the radiation field is relaxed to a steady state, the local temperature and fractional ionization of the gas are found by solving the equations of thermal and ionization equilibrium. In addition to fully-ionized species, the following ions are included in the calculations: C III–VI, N III–VII, O III–VIII, Ne III–X, Mg III–XII, Si IV–XIV, S IV–XVI, and Fe VI–XXVI. Elemental abundances are taken from Morrison & McCammon (1983). Ross & Fabian (2005) have summarized the atomic data employed. In particular, it should be noted that three-body recombination, which can be important for elements lighter than iron at the high densities in our models, is included in the recombination rate tables of Summers (1974) that are employed. Three-body recombination of iron is neglected, since it is only important at higher densities ($n_{\rm e} \gtrsim 10^{22}\,{\rm cm}^{-3}$) than occur in our models (Jacobs et al. 1977).

The density structure of the gas within the surface layer is found from the condition for hydrostatic equilibrium:

$$-\frac{dP_{\rm gas}}{dz} - \frac{1}{3}\frac{du}{dz} - \frac{GM\rho}{R^3}z = 0, \qquad (3)$$

where $P_{\rm gas}$ is the gas pressure, ρ is the gas density, and u is the total radiation energy density. Details of the method have been described by Ballantyne et al. (2001).

2.2 Results

We consider an illuminated accretion-disc surface located at $R = 12R_{\rm g}$ when the accretion rate corresponds to $\varepsilon = 0.1$ times the Eddington limit. The blackbody radiation emerging from the disc then corresponds to a temperature such that $kT_{\rm BB} \approx 0.35\,{\rm keV}$. The outer surface is illuminated by a cutoff power-law spectrum with photon index $\Gamma = 2$ and e-folding energy $E_{\rm cut} = 300\,{\rm keV}$ for the high-energy exponential cutoff. For self-consistent results, photon energies ranging from 1 eV to 1 MeV are treated in the radiative transfer calculation. However, the illuminating spectrum, which is probably produced by Compton upscattering of disc radiation by a hot accretion-disc corona (e.g., Shapiro, Lightman & Eardley 1976; Haardt & Maraschi 1993; Dove, Wilms & Begelman 1997), cannot be expected to extend to extremely low energies. Therefore, the illuminating spectrum is given an abrupt low-energy cutoff at $E = 0.1\,{\rm keV}$. The illumination has a total flux $F_0 = 0.1F_{\rm disc}$, so that the thermal radiation dominates. (In the 2–20 keV range, the illuminating flux is 0.17 times the disc flux.)

The calculated temperature and density structures of the surface layer are shown in Figure 1. The thermal radiation from the disc below keeps the temperature high throughout the surface layer, and the external radiation causes the temperature to rise with decreasing Thomson depth for $\tau_{\rm T} \lesssim 1$. Elements lighter than iron are fully ionized throughout the surface layer. The disc radiation is too soft to ionize iron K-shell electrons, however, and Fe XXV dominates for $\tau_{\rm T} \gtrsim 1/3$. The gas density decreases steadily as $\tau_{\rm T}$ decreases. There is no abrupt change in temperature and density like that found when a cooler AGN accretion disc is illuminated (Nayakshin, Kazanas & Kallman 2000; Ballantyne et al. 2001; Różańska et al. 2002).

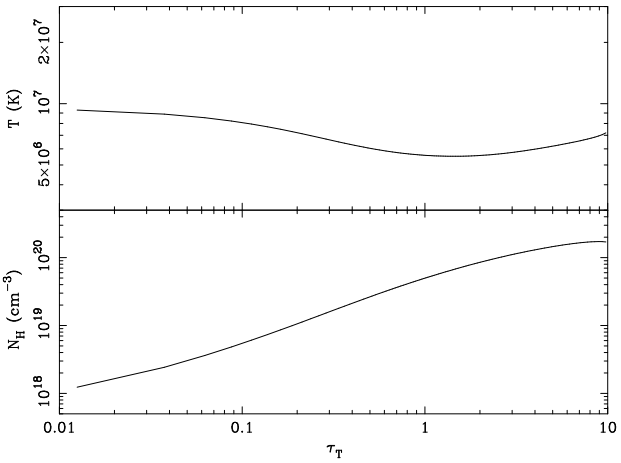

Figure 1. Temperature (top) and hydrogen number density (bottom) as functions of Thomson depth when the surface of a particular black-hole accretion disc at $R = 12R_{\rm g}$ is illuminated by a cutoff power-law spectrum with total flux $F_0 = 0.1F_{\rm disc}$.

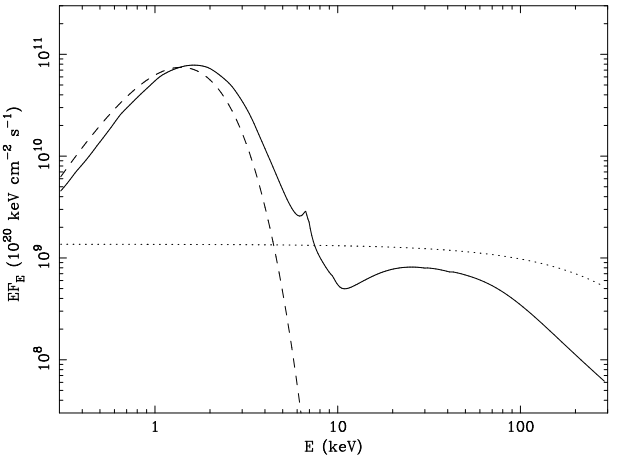

Figure 2. Spectrum (solid curve) emerging from the illuminated accretion-disk surface with the atmosphere in hydrostatic equilibrium. The blackbody spectrum entering the surface layer from below and the cutoff power-law spectrum illuminating the outer surface are represented by the dashed and dotted curves, respectively.

The spectrum emerging from the surface of the disc is shown in Figure 2. The hotter gas near the illuminated surface causes the 2–10 keV "thermal" spectrum to be enhanced both by Compton upscattering and by additional bremsstrahlung emission. The spectrum above 6 keV exhibits Compton-broadened Kα emission and K-absorption features due to Fe XXV. The characteristic "reflection hump" produced by Compton downscattering of high-energy photons is apparent at $E \sim 30\,{\rm keV}$.

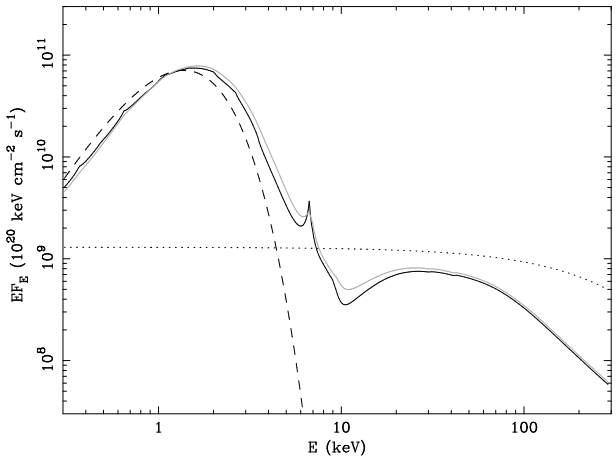

Figure 3. Constant-density reflection model. The darker solid curve shows the emerging spectrum when the thermal emission from the disc (dashed) has $kT_{\rm BB} = 0.35\,{\rm keV}$, while the illumination (dotted) has $\Gamma = 2$ and $F_0 = 0.1F_{\rm disc}$. For comparison, the lighter solid curve shows the spectrum from Fig. 2.

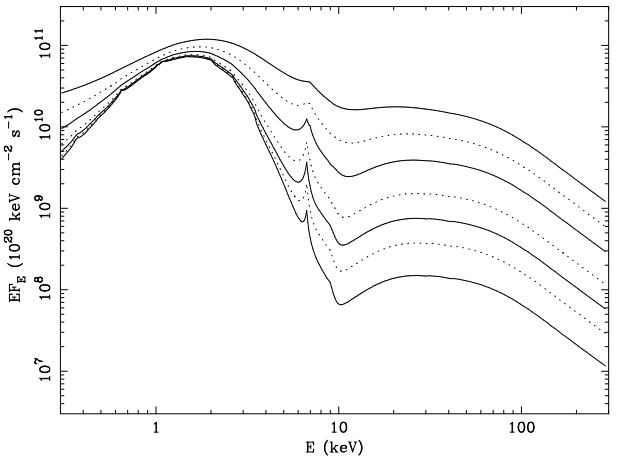

Figure 4. Emergent spectra when $F_0/F_{\rm disc} = 0.02$ (bottom solid curve), 0.05 (dotted), 0.1 (solid), 0.2 (dotted), 0.5 (solid), 1 (dotted) and 2 (top solid curve). Here $kT_{\rm BB} = 0.35\,{\rm keV}$ and $\Gamma = 2$ throughout.

3 CONSTANT-DENSITY MODELS

In reality, the detailed geometry and boundary conditions of the illuminated disc surface are poorly known. Therefore, it makes little sense to pursue hydrostatic-equilibrium models like the one presented in §2 any further. To study a range of reflection spectra that are possible, we simplify the situation by considering reflection by a constant-density atmosphere (see Ross & Fabian 2005). Indeed, Ballantyne et al. (2001) found that even under AGN conditions, models for reflection by atmospheres in hydrostatic equilibrium could be fitted by diluted (smaller reflection fraction) versions of constant-density reflection models.

The atmosphere of the accretion disc is approximated by a slab with fixed hydrogen density $n_{\rm H} = 10^{20}\,{\rm cm}^{-3}$ and Thomson depth $\tau_{\rm T} = 10$. The thermal emission from the disc is represented by a blackbody spectrum with designated temperature $T_{\rm BB}$ entering the slab from below. The outer surface is illuminated by a cutoff power-law spectrum with designated photon index Γ and $F_0/F_{\rm disc}$ ratio. The e-folding energy for the high-energy cutoff to the illumination is fixed at $E_{\rm cut} = 300\,{\rm keV}$, and the illumination again has a abrupt low-energy cutoff at $E = 0.1\,{\rm keV}$.

Figure 3 shows the emerging spectrum for a constant-density model with the same parameters as the hydrostatic-atmosphere model discussed previously, namely $kT_{\rm BB} = 0.35\,{\rm keV}$, $\Gamma = 2$, and $F_0/F_{\rm disc} = 0.1$. The constant density chosen corresponds to the density for $\tau_{\rm T} \gtrsim 1$ in the hydrostatic-atmosphere model, and the temperature in the constant-density model agrees well for $\tau_{\rm T} \gtrsim 1$. Since the density is higher for $\tau_{\rm T} \lesssim 1$, the effective ionization parameter is lower, and the gas is somewhat cooler and less highly ionized in the constant-density model. As a result, the Fe Kα line is slightly stronger, the iron K-edge is somewhat deeper, and at lower energies, tiny emission features are produced by recombinations to hydrogen-like ions of the lighter elements. Overall, however, the emergent spectrum is seen to be in reasonably good agreement with the result for an atmosphere in hydrostatic equilibrium.

The effect of modifying the total illuminating flux is shown in Figure 4. Of course, the thermal radiation becomes less dominant as the $F_0/F_{\rm disc}$ ratio increases. For the four lowest values of $F_0/F_{\rm disc}$ shown in Fig. 4, the illumination is so weak that the thermal radiation determines the ionization structure, with Fe XXV dominating throughout the atmosphere. For $F_0 = 0.5F_{\rm disc}$, however, the illumination has an ionization parameter $\xi_0 = 970\,{\rm erg\,cm\,s}^{-1}$, where

$$\xi_0 = \frac{4\pi F_0}{n_{\rm H}}. \qquad (4)$$

This makes Fe XXVI the dominant species near the illuminated surface ($\tau_{\rm T} \lesssim 0.4$), and Fe XXVI contributes significantly to the broad iron Kα line. For $F_0 = F_{\rm disc}$, iron is fully ionized for $\tau_{\rm T} \lesssim 0.4$, and Fe XXVI dominates for $0.4 \lesssim \tau_{\rm T} \lesssim 1.7$. Then Fe XXV and Fe XXVI together produce a particularly broad Kα blend. For $F_0 = 2F_{\rm disc}$ (top curve in Fig. 4), iron is fully ionized for $\tau_{\rm T} \lesssim 2$, and the iron Kα line has weakened.

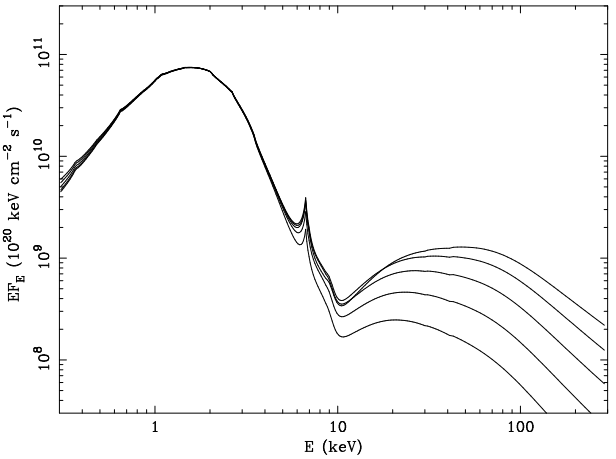

Figure 5. Emergent spectra when $\Gamma = 1.6$ (top curve at high photon energies), 1.8, 2.0, 2.2 and 2.4 (bottom curve at high photon energies). Here $kT_{\rm BB} = 0.35\,{\rm keV}$ and $F_0/F_{\rm disc} = 0.1$ throughout.

The effect of varying the power-law index Γ is shown in Figure 5. The main effect is on the high-energy tail above $\sim 10\,{\rm keV}$, where Compton downscattered illumination dominates the spectrum. For the steepest illuminating spectrum ($\Gamma = 2.4$), the 6–10 keV portion of the emergent spectrum is also lowered.

Finally, Figure 6 shows the effect of varying the blackbody temperature of the disc emission. For $kT_{\rm BB} = 0.25\,{\rm keV}$, the thermal emission is too soft and weak to keep heavier elements fully ionized. Here Mg XII, Si XIII–XIV, S XV, and Fe XXI–XXIII domi-

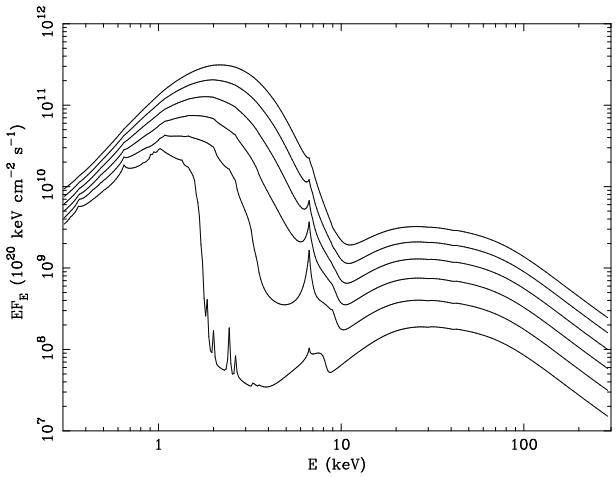

Figure 6. Emergent spectra when $kT_{\rm BB} = 0.25$ (bottom curve), 0.30, 0.35, 0.40, 0.45 and 0.50 keV (top curve). Here $\Gamma = 2$ and $F_0/F_{\rm disc} = 0.1$ throughout.

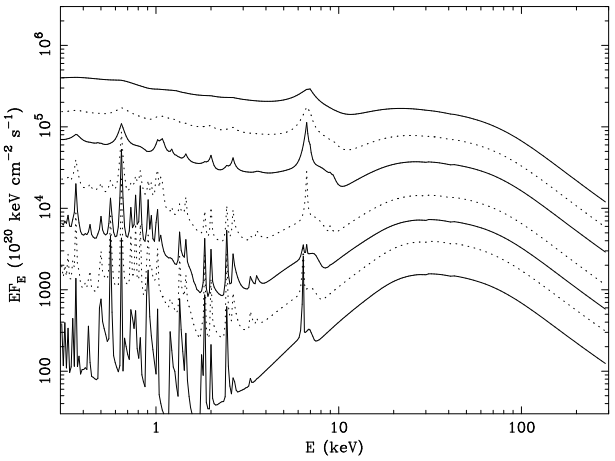

Figure 7. Constant-density reflection spectra under AGN conditions: the atmosphere has $n_{\rm H} = 10^{15}\,{\rm cm}^{-3}$, and the disc below is cold. Emergent spectra are shown for $\Gamma = 2$ illumination with the same ionization parameters as in Fig. 4, namely $\xi_0 = 38.8$ (bottom solid curve), 97.0 (dotted), 194 (solid), 388 (dotted), 970 (solid), 1940 (dotted), and 3880 erg cm s^{-1} (top solid curve).

nate for $\tau_{\rm T} \lesssim 1$. There is a steep dropoff in the emergent spectrum due to iron L-shell absorption, and Kα lines of Si XIII–XIV and S XV–XVI are visible. The iron Kα line is weak due to the destruction of these photons via the Auger effect during resonant trapping (see Ross, Fabian & Brandt 1996). For $kT_{\rm BB} = 0.30\,{\rm keV}$, S XVI and Fe XXV dominate near the illuminated surface, and the emergent spectrum exhibits a strong Fe XXV Kα line. As $kT_{\rm BB}$ increases beyond 0.35 keV, Fe XXV remains the dominant species in the atmosphere, but the iron Kα line becomes weaker and more difficult to distinguish from the strengthening thermal continuum.

4 DISCUSSION

In the high/soft state of a BHB, the X-ray spectrum is dominated by the soft thermal radiation, which generally accounts for $\gtrsim 75\%$ of the flux in the 2–20 keV range. Additional spectral components are generally a high-energy tail, which is approximately a power law with photon index $\Gamma \sim 2$, and a broad iron Kα emission feature (see Tanaka & Lewin 1995; Reynolds & Nowak 2003; McClintock & Remillard 2006; Remillard & McClintock 2006). We have demonstrated how illumination of a BHB accretion disc can help produce such features.

The emergent spectra under black-hole binary conditions are quite different than under the conditions in active galactic nuclei (AGN). For comparison, Fig. 7 shows the corresponding reflection spectra under conditions that would be expected in an active galactic nucleus. The density in the accretion-disc atmosphere and the total illuminating flux are lower, and thermal radiation from the cooler disc, which lies well below X-ray energies, is ignored. The models calculated have the same values for the illumination ionization parameter, ξ_0, as those shown in Fig. 4. With lower temperatures and little ionizing radiation within the disc, the metals are not highly ionized. For $\xi = 38.8$ and 97.0 erg cm s^{-1}, the atmosphere is only highly ionized in a very thin surface layer. Now the iron Kα emission is dominated by the 6.4-keV fluorescence of weakly ionized atoms. Strong emission features at lower energies are due to K-lines of the lighter elements as well as L-lines of iron, while the continuum there is suppressed by bound-free absorption. For $\xi = 194$ erg cm s^{-1}, the iron Kα line is weak due to resonant Auger destruction. For $\xi_0 = 388$ and 970 erg cm s^{-1}, the Fe XXV Kα line at 6.7 keV dominates, but strong emission lines are still present at lower energies. For $\xi = 1940$ and 3880 erg cm s^{-1}, the gas is highly ionized within a deep surface layer, and the reflected spectrum is fairly similar to the BHB case, except that the lack of soft thermal radiation makes the spectrum flatter for $E \lesssim 10\,{\rm keV}$.

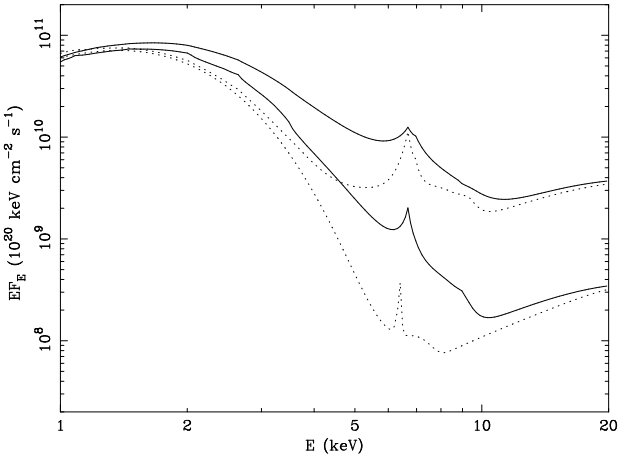

Figure 8. Solid curves show the emergent spectra for BHB models with $kT_{\rm BB} = 0.35\,{\rm keV}$, $\Gamma = 2$, and $F_0/F_{\rm disc}$ values of 0.05 (lower) and 0.50 (upper). Dotted curves show the result of adding a 0.35-keV blackbody spectrum to AGN reflection spectra with ξ_0 values of 97.0 (lower) and 970 erg cm s^{-1} (upper) that have been increased by a factor of 10^5.

In particular, reflection in a BHB system cannot be mimicked simply by adding a blackbody spectrum to the reflection spectrum from an otherwise cool disc. This is demonstrated in Figure 8, which shows two examples of adjusting a local AGN reflection spectrum upward by a factor of 10^5 and then adding a blackbody spectrum to represent the emission by the disc. For $\xi_0 = 97.0$ erg cm s^{-1}, the mimicked spectrum has a narrow iron line at 6.4 keV, while the actual BHB spectrum has a strong, Compton-broadened Fe XXV line (6.7 keV) atop a much higher continuum. For $\xi_0 = 970$ erg cm s^{-1}, on the other hand, the mimicked spectrum does have a broad Fe XXV line, but the actual BHB spec-

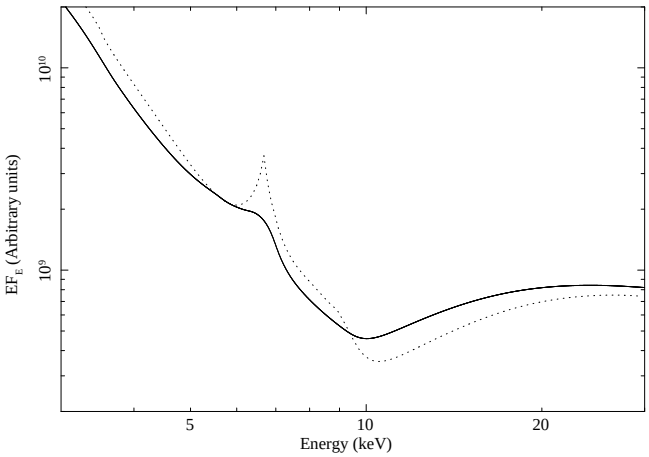

Figure 9. Effect of relativistic blurring on the reflected spectrum. A model with $kT_{\rm BB} = 0.35\,{\rm keV}$, $\Gamma = 2$, and $F_0/F_{\rm disc} = 0.1$ (dotted curve) has been blurred (solid curve) as if observed from a region with emissivity index 3 extending from 6 to 20 gravitational radii in a disc around a rotating black hole, and viewed at an inclination angle of 30°.

trum has a very different line shape due to a blend of Fe XXV and Fe XXVI emission, and the surrounding continuum is again higher.

If the accreting object was a neutron star ($M \approx 1.4 M_\odot$) instead of a 10-$M_\odot$ black hole, then both $F_{\rm disc}$ and $n_{\rm H}$ would be ~ 7 times larger for the same values of ε and $R/R_{\rm g}$. Although the "ionization parameter" of the disc radiation would be the same, its harder spectrum ($kT_{\rm BB}$ about 1.6 times larger) would give it greater ionizing power.

Of course, spectral features due to reflection by the inner portion of the accretion disc will be blurred by the relativistic Doppler effect and gravitational redshift. Figure 9 shows an example of such relativistic blurring for the model with $kT_{\rm BB} = 0.35\,{\rm keV}$, $\Gamma = 2$, and $F_0/F_{\rm disc} = 0.1$ discussed in §3. The Fe XXV Kα line, already broadened by Compton scattering, is further broadened and redshifted. The iron K-edge in the reflected spectrum is also smeared out, making it less prominent (see Ross et al. 1996). In this way it mimics the `smedge` model in XSPEC often used for fitting the spectra of BHB. This model is a simple phenomenological representation of a smeared absorption edge (Ebisawa et al. 1994), and has no clear physical basis.

Compton broadening of the iron Kα line is relatively more important for BHB at a given ξ_0 value than for AGN since the surface layers are hotter. This is important when deducing the spin of the black hole from the overall observed breadth of the line.

5 ACKNOWLEDGMENTS

We thank Jon Miller and an anonymous referee for helpful comments. RRR and ACF thank the College of the Holy Cross and the Royal Society, respectively, for support.

REFERENCES

Ballantyne D.R., Ross R.R., Fabian A.C., 2001, MNRAS, 327, 10
Bałucińska-Church M., Church M.J., 2000, MNRAS, 312, L55
Cooper G., 1971, Phys Rev D, 3, 2312
Davis S.W., Blaes O.M., Hubeny I., Turner N.J., 2005, ApJ, 621, 372
Davis S.W., Hubeny I., 2006, ApJ, 164, 530
Dove J.B., Wilms J., Begelman M.C., 1997, ApJ, 487, 747
Ebisawa K., et al., 1994, PASJ, 46, 375
Fabian A.C., Iwasawa K., Reynolds C.S., Young A.J., 2000, PASP, 112, 1145
George I.M., Fabian A.C., 1991, MNRAS, 249, 352
Guilbert P.W., Rees M.J., 1988, MNRAS, 233, 475
Haardt F., Maraschi L., 1993, ApJ, 413, 507
Jacobs V.L., Davis J., Kepple P.C., Blaha M., 1977, ApJ, 211, 605
Lightman A.P., White T.R., 1988, ApJ, 335, 57
Martocchia A., Matt G., Karas V., Belloni T., Feroci M., 2002, A&A, 387, 215
McClintock J.E., Remillard R.A., 2006, in Lewin W.H.G., van der Klis M., eds, Compact Stellar X-ray Sources. Cambridge University Press, Cambridge, p. 157
Merloni A., Fabian A.C., Ross R.R., 2000, MNRAS, 313, 193
Miller J.M. et al., 2002a, ApJ, 570, L69
Miller J.M., Fabian A.C., in 't Zand J.J.M., Reynolds C.S., Wijnands R., Nowak M.A., Lewin W.H.G., 2002b, ApJ, 577, L15
Miller J.M. et al., 2002c, ApJ, 578, 348
Miller J.M. et al., 2004, ApJ, 606, L131
Miller J.M., Homan, J., Steeghs, D., Rupen, M., Hunstead, R. W., Wijnands, R., Charles, P. A., Fabian, A. C., 2006, ApJ, 653, 525
Miller J.M. 2007, ARAA, astro-ph/07050540
Miniutti G., Fabian A.C., Miller J.M., 2004, MNRAS, 351, 466
Morrison R., McCammon D., 1983, ApJ, 270, 119
Nayakshin S., Kazanas D., Kallman T.R., 2000, ApJ, 537, 833
Remillard R.A., McClintock J.E., 2006, ARA&A, 44, 49
Reynolds C.S., Nowak M.A., 2003, PhysRept, 377, 389
Ross R.R., Fabian A.C., 1993, MNRAS, 261, 74
Ross R.R., Fabian A.C., 2005, MNRAS, 358, 211
Ross R.R., Fabian A.C., Brandt W.N., 1996, MNRAS, 278, 1082
Rossi S., Homan J., Miller J.M., Belloni T., 2005, MNRAS, 360, 763
Różańska A., Dumont A.-M., Czerny B., Collin S., 2002, MNRAS, 332, 799
Shakura N.I., Sunyaev R.A., 1973, A&A, 24, 337
Shapiro S.L., Lightman A.P., Eardley D.M., 1976, ApJ, 204, 187
Shimura T., Takahara F., 1995, ApJ, 445, 780
Summers H.P., 1974, Appleton Laboratory, Internal Memo 367
Tanaka Y., Lewin W.H.G., 1995, in Lewin W.H.G., van Paradijs J., van den Heuvel E.P.J., eds, X-ray Binaries. Cambridge University Press, Cambridge, P. 126

This paper has been typeset from a TEX/ LATEX file prepared by the author.